Intracellular Mg^{2+} interacts with structural determinants of the narrow constriction contributed by the NR1-subunit in the NMDA receptor channel

Lonnie P. Wollmuth, Thomas Kuner* and Bert Sakmann

Abteilung Zellphysiologie and **Abteilung Molekulare Neurobiologie, Max-Planck-Institut für medizinische Forschung, Jahnstrasse 29, D-69120 Heidelberg, Germany*

(Received 10 January 1997; accepted after revision 12 September 1997)

1. *N*-methyl-D-aspartate (NMDA) receptor channels are blocked by intracellular Mg^{2+} in a voltage-dependent manner. Amino acid residues positioned at or near the narrow constriction that interact with intracellular Mg^{2+} were identified in recombinant NR1–NR2A channels expressed in *Xenopus* oocytes or human embryonic kidney (HEK) 293 cells.

2. In the absence of extracellular Ca^{2+}, the block of wild-type channels by intracellular Mg^{2+} measured using macroscopic currents showed a voltage dependence (δ) of around 0·38 and a voltage-independent affinity for the channel of 4 mM. These parameters were independent of the Mg^{2+} concentration (0·05–10 mM), and were indistinguishable from those found for the reduction of single channel amplitudes under the same ionic conditions. Under biionic conditions with high intracellular Mg^{2+} and K^+ extracellularly, Mg^{2+} was weakly permeant. Mg^{2+} efflux, however, attenuated the block only at positive potentials (> +80 mV).

3. Substitutions of the N-site asparagine in the NR1-subunit altered intracellular Mg^{2+} block over physiological membrane potentials (+10 to +50 mV). Substitution of glycine, glutamine or serine attenuated the extent of block whereas the negatively charged aspartate enhanced it, consistent with the side chain of the native asparagine at this position contributing to a blocking site for intracellular Mg^{2+}.

4. Substitutions of the N-site or N + 1 site asparagine in the NR2A-subunit, which form a blocking site for extracellular Mg^{2+}, also altered the block by intracellular Mg^{2+}. However, for the NR2A-subunit N-site asparagine, the block was reduced but only at non-physiological high potentials (> +70 mV).

5. The NR2A-subunit N + 1 site asparagine, which together with the NR1-subunit N-site asparagine forms the narrow constriction of the channel, also contributed to a blocking site for intracellular Mg^{2+}. However, it did so to a lesser extent than the NR1-subunit N-site and in a manner different from its contribution to a blocking site for extracellular Mg^{2+}.

6. It is concluded that intracellular Mg^{2+} interacts with residues that form the narrow constriction in the NMDA receptor channel with the N-site asparagine of the NR1-subunit representing the dominant blocking site. Thus, intracellular Mg^{2+} interacts with different asparagine residues at the narrow constriction than extracellular Mg^{2+}, although the two blocking sites are positioned very close to each other.

In addition to being blocked by extracellular Mg^{2+}, *N*-methyl-D-aspartate (NMDA) receptor channels are also blocked by intracellular Mg^{2+} (Johnson & Ascher, 1990; Li-Smerin & Johnson, 1996*a*). The block by extracellular Mg^{2+} is critical physiologically allowing the NMDA receptor channel to function as a coincidence detector of pre- and postsynaptic activity (e.g. Bliss & Collingridge, 1993). In contrast, the physiological function of the block by intracellular Mg^{2+} is unknown. Mg^{2+} block from either side of the membrane is voltage dependent but more so from the outside. Extracellular Mg^{2+} gives an apparent site of interaction between 0·8 and 1 across the transmembrane electric field (Ascher & Nowak, 1988; Jahr & Stevens, 1990) whereas from the inside it is around 0·35 (Johnson & Ascher, 1990). As pointed out by Johnson & Ascher (1990), the overlap in the positioning of apparent blocking sites for intracellular and extracellular

Mg^{2+} complicates definition of the mechanism of the block. Identification of residues contributing to intracellular Mg^{2+} block and their relationship to that by extracellular Mg^{2+} could clarify the positioning of the blocking site for extracellular Mg^{2+}.

In the NMDA receptor channel, the narrow constriction or selectivity filter is formed near the tip of the loops arising from the M2 segments of the NR1- and NR2-subunits (Kuner, Wollmuth, Karlin, Seeburg & Sakmann, 1996). Two asparagine residues, one occupying the N-site in the NR1-subunit and the other the non-homologous N + 1 site in the NR2A-subunit, are major determinants of this structure (Wollmuth, Kuner, Seeburg & Sakmann, 1996). The N-site and N + 1 site asparagines in the NR2A-subunit contribute significantly to a blocking site for extracellular Mg^{2+} (Burnashev *et al.* 1992; Mori, Masaki, Yamakura & Mishina, 1992; Sakurada, Masu & Nakanishi, 1993; Wollmuth, Kuner & Sakmann, 1998). On the other hand, the N-site asparagine in the NR1-subunit is less important for extracellular Mg^{2+} block but is critical for Ca^{2+} permeation (Burnashev *et al.* 1992). Recent studies examining the block by impermeant organic cations indicated that the voltage dependence of the block by intracellular organic cations (Villarroel, Burnashev & Sakmann, 1995; Zarei & Dani, 1995) and intracellular Mg^{2+} is similar suggesting that intracellular Mg^{2+} may block NMDA receptors at the narrow constriction. To test this idea, we examined how substitutions of residues exposed to the lumen and positioned at or near the narrow constriction affect intracellular Mg^{2+} block. We report that intracellular Mg^{2+}, like extracellular Mg^{2+}, interacts with structural elements defining the narrow constriction. However, in contrast to extracellular Mg^{2+}, this interaction primarily occurs with the N-site of the NR1-subunit rather than with the two adjacent asparagines in the NR2A-subunit.

METHODS

Heterologous expression of NMDA receptor channels

NR1 mutants were co-expressed with wild-type NR2A or vice versa in *Xenopus* oocytes and human embryonic kidney 293 cells (HEK 293) (Wollmuth *et al.* 1996). *Xenopus* oocytes were taken from frogs anaesthetized in an ice bath containing 0·3 % MS-222 for 40 min. Giant inside-out macropatches (Hilgemann, 1995) were isolated 3–8 days after injection. Mutated positions are identified by defining the N-site as position '0' (Kuner *et al.* 1996): the NR1-subunit N-site (position 598 in the mature protein) is identified as NR1(N0); in the NR2A-subunit, the N-site (position 595), the adjacent asparagine (position 596) and the serine (position 597) are NR2A(N0), NR2A(N + 1) and NR2A(S + 2), respectively.

Solutions

For giant inside-out patches (bath applied) and for whole-cell recordings of HEK 293 cells (pipette solution), the intracellular solution consisted of (mM): 100 KCl, 10 Hepes and 10 EGTA; pH adjusted to 7·2 with KOH. $MgCl_2$ was added to this solution to yield the free Mg^{2+} concentration indicated in the text (Moisescu & Thieleczek, 1978; Stephenson & Thieleczek, 1986). For giant inside-out patches, the extracellular (pipette) solution consisted of (mM): 100 KCl, 10 Hepes and 10 EDTA; pH adjusted to 7·2 with KOH, to which 100 μM glutamate and 10 μM glycine were added. Outward Mg^{2+} permeability was measured in HEK 293 cells with the pipette solution containing (mM): 78 $MgCl_2$, 2 $Mg(OH)_2$ and 10 Hepes, with the final pH 7·2; and the extracellular solution (mM): 100 KCl and 10 Hepes, pH adjusted to 7·2 with KOH. The Mg^{2+} salts were of ultrapure grade (Merck, Darmstadt, Germany).

Current recordings and data analysis

Currents were recorded at room temperature (19–23 °C) using an EPC-9 amplifier with PULSE software (HEKA electronics GmbH, Lambrecht, Germany), low-pass filtered at 100 Hz (voltage ramps) or 500 Hz (voltage steps), and digitized at 1 kHz. Pipettes had resistances of 150–400 kΩ (giant inside-out) or 1–2 MΩ (whole-cell) when filled with the pipette solution and measured in the K^+ solution. Giant inside-out patch electrodes were dipped in liquid paraffin and washed with distilled water (Hilgemann, 1995). Bath solutions were applied using a Piezo-driven double-barrel application system. For giant inside-out patches, only the total current could be measured (2–15 nA at +100 mV) since the pipette continuously contained glutamate and glycine; we assumed that the total current was predominantly carried by NMDA receptor channels since in five patches without glutamate and glycine in the pipette, the seal resistance was always greater than 2 GΩ producing a leak current of at most 50 pA at +100 mV. Currents in the presence of Mg^{2+}, where the estimated leak current was more than 10 % of the total current (assuming the seal resistance was 2 GΩ), were not analysed. To correct for drift and junction potentials, control recordings (symmetrical [KCl], no Mg^{2+}) measured before and after an application of Mg^{2+} were shifted along the axis to cross 0 mV. This shift was normally less than ±2 mV and was used to shift the intervening record in the presence of Mg^{2+}. For wild-type and all mutant channels, current amplitudes produced by voltage ramps made from either positive to negative potentials or vice versa in the presence or absence of Mg^{2+} were indistinguishable. All curve fitting was done using Igor Pro (WaveMetrics, Inc., Lake Oswego, OR, USA). Unless indicated otherwise, results are reported in the text as means ± S.E.M. and shown graphically as means ± 2 S.E.M.

Single channel analysis. Single channel recordings were made with an EPC-7 amplifier (HEKA electronics GmbH). Patch pipettes were pulled from borosilicate glass coated with Sylgard 184 resin (Dow Corning, MI, USA) and fire polished to a final resistance of 8–12 MΩ. Patches were isolated from HEK 293 cells in the inside-out configuration (10 μM glycine and 1 μM glutamate in the patch pipette). The intracellular (100 mM KCl, 10 mM EGTA, 10 mM Hepes) and extracellular (100 mM KCl, 10 mM EDTA, 10 mM Hepes) solutions were identical to those used to record giant inside-out patch currents except that 0·5 mM EDTA was added to the intracellular solution in the control recording to remove any residual Mg^{2+}. Single channel currents were recorded on a digital tape recorder (DTR-1205; BioLogic, Cliax, France) and were filtered at 1 kHz (−3 dB, 8-pole Bessel) and digitized at 5 kHz (Aquire, SKALAR Instruments, Inc., Seattle, WA, USA; or CED 1401 interface). Individual currents were fitted using either Tac single channel analysis program (SKALAR Instruments, Inc.) or by the time-course fitting procedure with software kindly provided by David Colquhoun (University College London, UK). Unless otherwise noted, mean unitary current amplitudes were determined from maximum likelihood fits of Gaussian distributions to open point amplitude histograms. Only openings longer than 2 filter rise times were included in the amplitude distributions to minimize the inclusion of false events.

Table 1. Woodhull parameters for block of wild-type NR1–NR2A channels by intracellular Mg^{2+} in symmetrical [KCl]

$[Mg^{2+}]$ (mM)	δ	$K_{0.5}$(0 mV) (mM)	n
0·05	0·39 ± 0·02	4·1 ± 0·7	5
0·1	0·37 ± 0·01	3·9 ± 0·2	8
0·3	0·39 ± 0·01	3·8 ± 0·2	8
1	0·38 ± 0·01	4·0 ± 0·2	7
3·6	0·37 ± 0·01	4·2 ± 0·1	9
10	0·36 ± 0·01	4·3 ± 0·3	4
20	—*	—*	4
50	—*	—*	5

Solutions: intracellular (mM): 123·5 KCl, 10 Hepes, 10 EGTA; extracellular (mM): 123·5 KCl, 10 Hepes, 10 EDTA. $MgCl_2$ was added to the intracellular solution to obtain the free Mg^{2+} concentration. Parameters were derived by fitting the linear part of plots of $\ln(I_B/(I_0 - I_B))$ against voltage (eqn (2); see Fig. 1*C*). Except for 0·05 and 0·1 mM (+40 to +100 mV) and 10 mM (+10 to +60 mV), all fits were from +10 to +80 mV. For 10 mM a 2 GΩ leak was also assumed. * Parameters were not determined because the block was too strong. Values are means ± S.E.M.

Mg^{2+} permeability. Mg^{2+} permeability in NMDA receptor channels measured with high intracellular Mg^{2+} was estimated by determining the reversal potential for glutamate-activated currents with 80 mM $MgCl_2$ in the pipette and 103·5 mM KCl extracellularly. The liquid junction potential between the 103·5 mM K^+ and 80 mM $MgCl_2$ solutions (pipette) was +10·2 mV (pipette positive). To ensure equilibration between the pipette and intracellular contents, we used large-sized pipettes (1–2 MΩ), typically giving access resistances between 2 and 6 MΩ, and recorded reversal potentials at least 5 min after break-in. For mutant channels, this index of Mg^{2+} permeability was of limited quantitative value since it requires the assumption that the substitutions have no effect on K^+ permeation, a situation that probably does not hold. We therefore refer to this parameter as apparent permeability.

Voltage-dependent block. To model the relative location of a blocking site for Mg^{2+}, we assumed that Mg^{2+} acts within the transmembrane electric field. With a Woodhull model (Woodhull, 1973), the current amplitude in the presence (I_B) and absence (I_0) of Mg^{2+} are related according to the relationship:

$$I_B = \frac{I_0}{1 + \dfrac{[Mg^{2+}]_i}{K_{0.5}(0\text{ mV})\exp\left(\dfrac{-z\delta EF}{RT}\right)}}, \quad (1)$$

where $K_{0.5}$(0 mV) is the half-maximal block at 0 mV, δ is the portion of the membrane electric field sensed by the site and z is the valence of the blocking ion. R, T and F have their normal thermodynamic meanings and the quantity RT/F was 25·4 mV. For individual Mg^{2+} concentrations, we determined $K_{0.5}$(0 mV) and δ by fitting a linear equation to $\ln(I_B/(I_0 - I_B))$ plotted against voltage (DiFrancesco, 1982) where $\ln(I_B/(I_0 - I_B))$ is defined as:

$$\ln(I_B/(I_0 - I_B)) = -z\delta FE/RT - \ln([Mg^{2+}]_i/K_{0.5}(0\text{ mV})). \quad (2)$$

Alternatively, the Woodhull parameters were quantified by determining the concentration dependence of the fraction blocked ($1 - I_B/I_0$) at a constant potential and plotting $K_{0.5}$ against potential according to the relationship (Wollmuth, 1994):

$$\ln(K_{0.5}(E)) = \ln(K_{0.5}(0\text{ mV})) + z\delta FE/RT. \quad (3)$$

RESULTS

Block of wild-type NR1–NR2A channels by intracellular Mg^{2+}

Figure 1*A* shows block by intracellular Mg^{2+} of the total current produced by voltage ramps in a giant inside-out patch isolated from an oocyte expressing NR1–NR2A subunits and recorded in symmetrical $[K^+]$ with 0 extracellular Ca^{2+}. In the absence of Mg^{2+}, the current–voltage relationship was linear. When Mg^{2+} (0·1–10 mM) was added to the intracellular solution, the outward current was reduced in a concentration- and voltage-dependent manner. Figure 1*B* shows plots of the fraction of channels blocked, $1 - I_B/I_0$. The block by intracellular Mg^{2+} differed from that by extracellular Mg^{2+} in that the voltage-dependent region occurred at positive potentials and was not as steep. We quantified the block by transforming the blocked current into a linear form (eqn (2); Fig. 1*C*). Over intermediate potentials, these plots showed a linear region consistent with a Woodhull model (Woodhull, 1973). The steepness of the fitted line, which is an index of the voltage dependence of the block, δ, did not depend on Mg^{2+} concentration. Indeed, as summarized in Table 1, the voltage dependence of the block by Mg^{2+}, around 0·38, was independent of concentration from 0·05 to 10 mM, as was the voltage-independent affinity for the channel, $K_{0.5}$(0 mV), which was around 4 mM. These results suggest that intracellular Mg^{2+} acts as a simple blocker at potentials between +10 and +80 mV.

After establishing the concentration independence of the block parameters for individual concentrations, we used a second approach to quantify the block by intracellular Mg^{2+} (Fig. 2). Figure 2*A* shows the reduction of current at three different potentials as a function of the Mg^{2+} concentration with the continuous lines being fitted Langmuir isotherms.

As expected for a voltage-dependent block mechanism, the half-maximal block, $K_{0.5}$, showed a higher affinity at more positive potentials, increasing from 2·2 mM at +20 mV to 0·34 mM at +80 mV. A plot of $K_{0.5}$ at different membrane potentials (Fig. 2*B*) shows a region of linearity, from +10 to +80 mV. The fitted line (eqn (3)) give a voltage dependence of the block, δ, of 0·39 ± 0·01 and a voltage-independent affinity for the channel, $K_{0.5}$(0 mV), of 4·1 ± 0·1 mM. Hence, this alternative approach to quantifying block, which is more rigorous since it is based on a wide concentration range, yielded values indistinguishable from those determined for individual concentrations.

The results shown in Figs 1 and 2, which are based on macroscopic NMDA receptor currents, suggest that between +10 and +80 mV the reduction of current by intracellular Mg^{2+} is a simple block mechanism. Nevertheless, previous results have indicated that in addition to a block or occlusion mechanism (i.e. reduction of single channel amplitudes), intracellular Mg^{2+} also increases the open probability of native NMDA receptor channels in cultured rat neurons (Li-Smerin & Johnson, 1996*b*). Macroscopic currents in the presence of Mg^{2+} would therefore be the net effect of a decrease in single channel amplitude and an increase in open probability. The latter action makes the apparent block of macroscopic currents weaker than that for the reduction of single channel amplitudes. To test directly the relationship between single channel and macroscopic currents, we quantified the reduction of single channel current amplitudes by intracellular Mg^{2+} of recombinant NR1–NR2A channels (Fig. 3).

Figure 3*A* illustrates example NR1–NR2A single channels at +50 mV in symmetrical [KCl] with 0 external Ca^{2+}. In the absence of Mg^{2+} (upper trace), the channels opened to a single level with a mean unitary amplitude of 2·95 pA

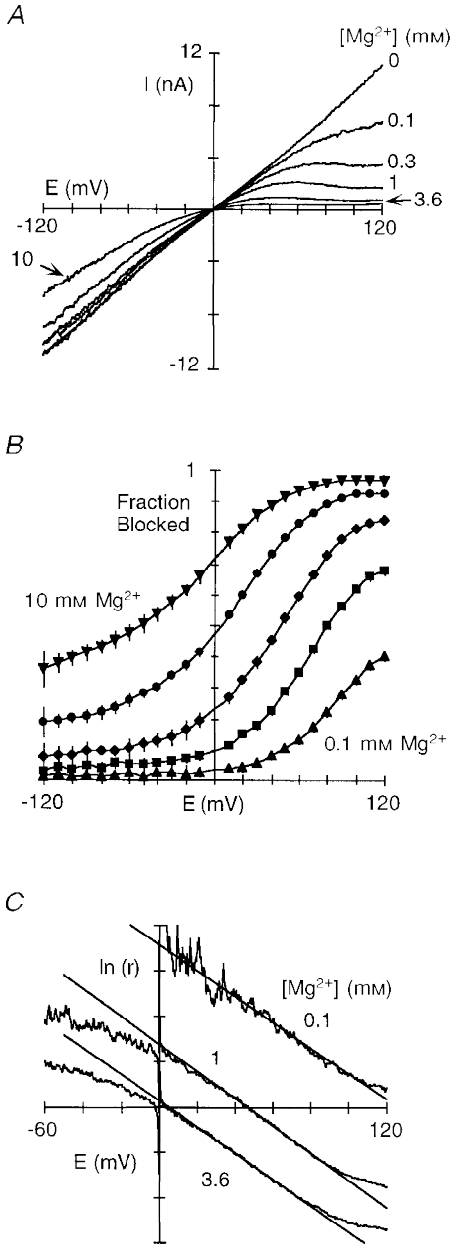

Figure 1. Block of wild-type NR1–NR2A channels by intracellular Mg^{2+}

A, Mg^{2+} block recorded in giant inside-out patches isolated from *Xenopus* oocytes expressing wild-type NR1- and NR2A-subunits. Currents were generated by voltage ramps (~80 mV s^{-1}) and were recorded in symmetrical [KCl] with the pipette solution containing 100 μM glutamate and 10 μM glycine (see Methods). *B*, mean fraction blocked, $1 - I_B/I_0$, where I_0 is the current amplitude in the absence and I_B the amplitude in the presence of different Mg^{2+} concentrations. Each point is shown as the mean ± 2 S.E.M. and corresponds to Mg^{2+} concentrations of 0·1 (▲), 0·3 (■), 1 (◆), 3·6 (●), and 10 mM (▼). Continuous curves have no theoretical significance. *C*, $\ln(I_B/(I_0 - I_B))$ (eqn (2)), referred to as $\ln(r)$, plotted against voltage for three different Mg^{2+} concentrations. Lines were fitted over the apparent linear region from +40 to +100 mV (0·1 mM Mg^{2+}) and +10 to +80 mV (1 and 3·6 mM Mg^{2+}).

(Fig. 3*B*). In the presence of intracellular Mg^{2+} (1 mM; Fig. 3*A*, lower trace), the single channel amplitude was reduced, reflecting the fact that the block by intracellular Mg^{2+} occurs so rapidly that the individual blocking events cannot be resolved (e.g. Johnson & Ascher, 1990). The unitary amplitude in Mg^{2+} was 1·42 pA (Fig. 3*C*), yielding a fraction blocked of, on average, 0·50 ± 0·02 ($n = 5$ patches), a value comparable to that obtained using macroscopic currents at the same potential (0·52 ± 0·01, $n = 7$; Fig. 1*B*). Figure 3*D* shows NR1–NR2A single channel current amplitudes measured over a wide voltage range. The slope conductance of these amplitudes in the absence of Mg^{2+} (filled circles) was not symmetrical being greater at potentials negative to the reversal potential (75 ± 2 pS) than at positive potentials (54 ± 1 pS, $n = 4$). In contrast, macroscopic currents showed a nearly linear current–voltage relationship (Fig. 1*A*); this channel difference in the shape of the current–voltage relationship between single channel amplitudes and macroscopic currents is presumably due to an increased open probability of NMDA receptor channels with positive potentials (Nowak & Wright, 1992). Nevertheless, as shown in Fig. 3*E*, intracellular Mg^{2+} reduced single channel amplitudes (open circles) to an extent that was indistinguishable from that for macroscopic currents (filled circles). In addition, a Woodhull analysis of the reduction of single channel amplitudes yielded a δ of 0·37 ± 0·02 and a $K_{0\cdot5}$(0 mV) of 4·3 ± 0·3 mM ($n = 4$; Fig. 3*D*, continuous line through points in Mg^{2+}). Quantitatively, the $K_{0\cdot5}$(0 mV) measured using single channel amplitudes must be viewed cautiously since the fit was extrapolated from +30 to 0 mV. Nevertheless, the similarity between the block measured using macroscopic currents and the reduction of single channel amplitudes suggests that the primary action of intracellular Mg^{2+} on macroscopic currents under our conditions is an occlusion mechanism.

In summary, a Mg^{2+}-dependent increase in NMDA receptor channel open probability does not appear significant under our recording conditions. The basis for this difference from prior reports is unknown (see Discussion). Nevertheless, additional evidence consistent with the idea that the block of macroscopic currents by intracellular Mg^{2+} primarily reflects an occlusion process is that the block parameters derived from macroscopic currents show no concentration dependence (Table 1), a result also found for the reduction of single channel amplitudes (Johnson & Ascher, 1990; Li-Smerin & Johnson, 1996*a*).

Intracellular Mg^{2+} permeates wild-type NR1–NR2A channels

For macroscopic currents, three regions of block of NMDA receptor channels by intracellular Mg^{2+} were discernible (see Fig. 2*B*). Between +10 and +80 mV the block followed a simple Woodhull model. On the other hand, at potentials negative to 0 mV and positive to +80 mV, the block deviated from this model. At negative potentials, Mg^{2+} attenuated the inwardly directed current more than that predicted by the voltage-dependent parameters suggesting that intracellular Mg^{2+} may act not only deep within the pore but also at positions near the intracellular mouth of the channel. At potentials > +80 mV, the block was weaker than expected. This deviation reflects the fact that intracellular Mg^{2+} acts as a permeant blocker. As shown in Fig. 4*A*, the amplitude of the glutamate-activated currents recorded in HEK 293 cells with 0·3 mM Mg^{2+} in the pipette reached a plateau between +90 and +130 mV and then increased at more positive potentials. Such behaviour is typical of a blocking ion that occludes the pore at intermediate potentials but passes through the channel at extreme potentials. To estimate permeability for intracellular Mg^{2+}, we determined the reversal potential of glutamate-activated currents in HEK 293 cells with 80 mM $MgCl_2$ in the pipette and 103·5 mM KCl extracellularly. For wild-type

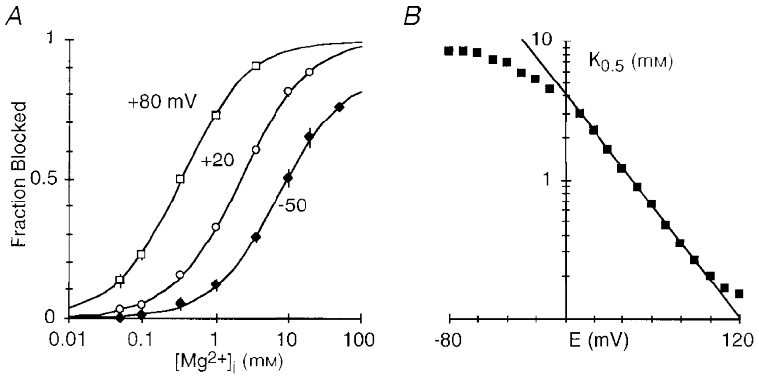

Figure 2. Voltage dependence of intracellular Mg^{2+} block of wild-type NR1-NR2A channels

A, mean fraction blocked, $1 - I_B/I_0$, in the presence (I_B) or absence (I_0) of Mg^{2+} at different membrane potentials. Continuous curves are fitted Langmuir isotherms ($1/(1 + K_{0\cdot5}(E)/[Mg^{2+}]_i)$) with $K_{0\cdot5}$ values of 0·34 mM (+80 mV), 2·2 mM (+20 mV) and 7·3 mM (−50 mV). *B*, $K_{0\cdot5}$ as a function of membrane potential with the straight line a linear equation fit from +10 to +80 mV (eqn (3)).

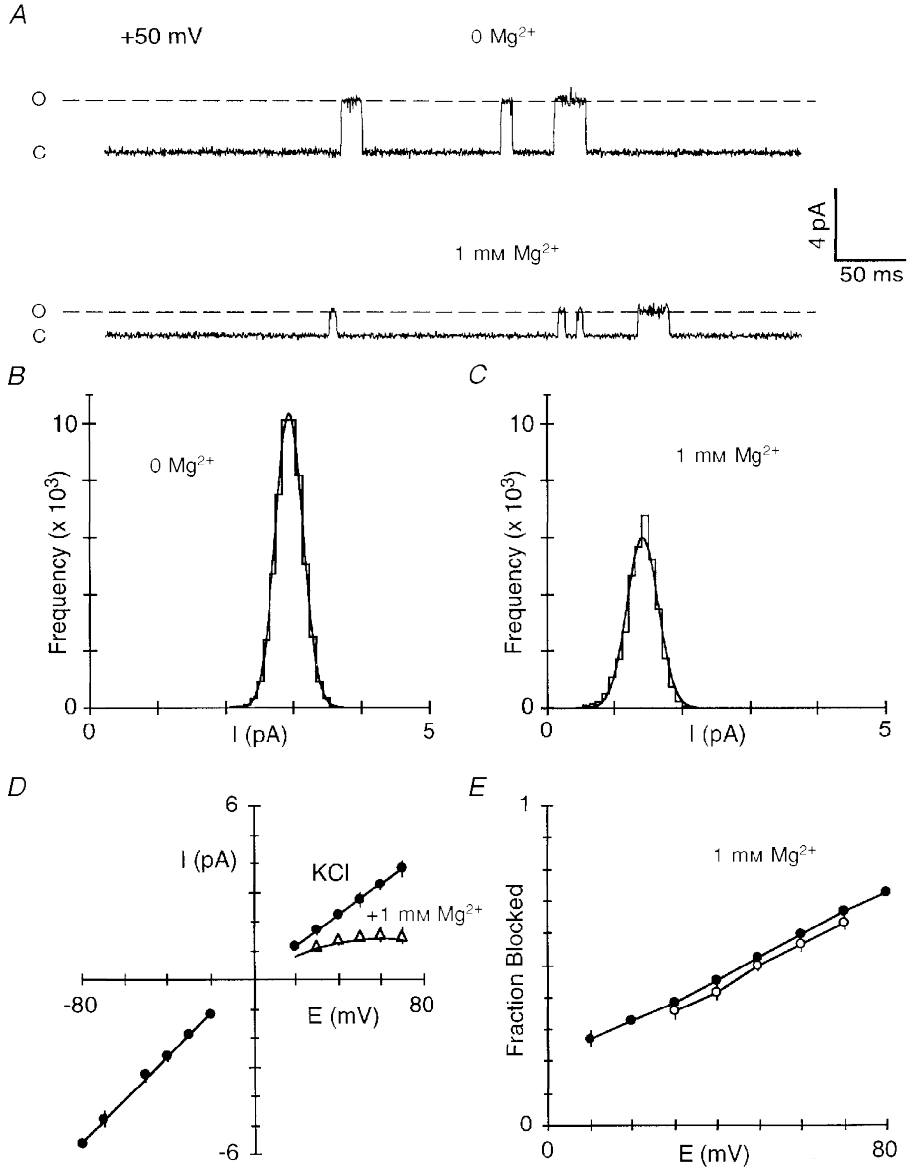

Figure 3. Reduction of wild-type NR1–NR2A single channel amplitudes by intracellular Mg^{2+}

A, example single channel currents at +50 mV in the absence (upper trace) or presence (lower trace) of 1 mM Mg^{2+} applied to the intracellular face. Traces are from the same inside-out patch isolated from a HEK 293 cell expressing wild-type NR1–NR2A channels. O, open; C, closed. *B* and *C*, open point amplitude histograms in the absence (*B*) or presence (*C*) of 1 mM intracellular Mg^{2+} for the patch in *A*. Bin width was 0·1 pA. Continuous curves are maximum likelihood fits of Gaussian distributions. In 0 Mg^{2+}, the mean unitary amplitude was 2·95 ± 0·20 pA (mean ± S.D.) whereas in 1 mM Mg^{2+} it was 1·42 ± 0·23 pA. *D*, example NMDA receptor single channel current amplitudes as a function of voltage in the absence (●) or presence (△) of 1 mM intracellular Mg^{2+}. Amplitudes are the mean of at least 50 events at each potential. Lines through the filled circles are fitted linear equations yielding slope conductances of 74 pS (negative limb) and 54 pS (positive limb). The mean reversal potential determined from fourth-order polynomial fits to the currents in the absence of Mg^{2+} was −1·3 ± 1·2 mV ($n = 4$). Current amplitudes were not measured at potentials positive to +70 mV due to patch instability. The continuous line through the points in Mg^{2+} is from eqn (1) using I_0 based on the single channel amplitudes and the mean Woodhull parameters ($\delta = 0{\cdot}37 \pm 0{\cdot}02$, $K_{0\cdot5}(0\text{ mV}) = 4{\cdot}3 \pm 0{\cdot}3$ mM; $n = 4$) derived from the reduction of single channel amplitudes and using eqn (2). *E*, mean fraction blocked, $1 - I_B/I_0$, in 1 mM Mg^{2+} measured using macroscopic currents (●) or the reduction of single channel amplitudes (○). Each point is shown as the mean ± 2 S.E.M. The lines have no theoretical significance.

(Fig. 4*B*), the current reversed direction from inward to outward at +56 ± 0·5 mV ($n = 5$), which is comparable to the ~51 mV change in the reversal potential for extracellular Mg^{2+} (Wollmuth *et al.* 1998). However, since the voltage dependence of the block does not depend on Mg^{2+} concentration or the voltage range over which the block was quantified, at least up to +80 mV, permeation by intracellular Mg^{2+} does not contribute significantly to the mechanism of block at physiological potentials (see also Li-Smerin & Johnson 1996*a*). Analysis of block and permeation in mutant channels further supports this idea.

The N-site asparagine in the NR1-subunit contributes to a blocking site for intracellular Mg^{2+} over physiological potentials

In considering how residues contribute to a blocking site, we initially examined the substitution of the small and non-polar glycine; this substitution removes any structural and energetic contribution a polar side chain would make to a blocking site and therefore would presumably attenuate the block. A comparison of block by intracellular Mg^{2+} in channels containing glycine (G) substituted for any one of three asparagine residues positioned at (NR1(N0), NR2A(N + 1)) or external to (NR2A(N0)) the narrow constriction is shown in Fig. 5*A*–*C*. As shown in Fig. 6*A*, their effect on the block, in comparison to that in wild-type (filled circles), depended strongly on membrane potential. In NR1(N0G) channels (open squares), the extent of block was attenuated over the entire voltage range with a much stronger relative attenuation at positive potentials. As analysed in Fig. 6*B*, a component of the block remained voltage dependent in these channels over intermediate or physiological potentials (~+10 to +50 mV) but was reduced compared with wild-type from 0·38 to 0·28 as was the $K_{0.5}$(0 mV), from 4·1 to 5·2 mM (Table 2). This result is consistent with intracellular Mg^{2+} interacting with the native asparagine at this position over physiological potentials. In contrast, in NR2A(N0G) (open circles) and NR2A(N + 1G) (open triangles), the block was reduced relative to wild-type only at very positive potentials. Indeed, over physiological potentials, the block was somewhat enhanced (Fig. 6*B*). This reflects an increased voltage dependence (~0·45 for both) while leaving $K_{0.5}$(0 mV) essentially unchanged (~3·9 mM; Table 3). However, block in these NR2A mutant channels at positive potentials differed in that it was attenuated more strongly in NR2A(N + 1G), with this attenuation occurring at less positive potentials (at approximately +70 mV in NR2A(N + 1G) and at +90 mV in NR2A(N0G) relative to that for wild-type channels).

A comparison of the voltage dependence of the block by 0·3 and 3·6 mM Mg^{2+} for the NR1(N0G), NR2A(N0G) and NR2A(N + 1G) channels as well as NR2A(S + 2G) with that in wild-type is shown in Fig. 7. In no instance was the voltage dependence of the block concentration dependent. Further, in all NR2A-subunit glycine substitutions the voltage dependence of the block was enhanced. Hence, removing the side chain at NR2A(N0), NR2A(N + 1) or NR2A(S + 2) did not disrupt the block over physiological potentials, as if a site of interaction for intracellular Mg^{2+} remained intact. On the other hand, a similar substitution at NR1(N0) attenuated the block over the entire voltage range suggesting that this position contributes to a blocking site for intracellular Mg^{2+}.

In NR1(N0G)–NR2A channels, the reduction of single channel amplitudes by intracellular Mg^{2+} is attenuated

Given that substitutions at NR1(N0) can have strong effects on single channel behaviour (e.g. Premkumar & Auerbach, 1996; Schneggenburger & Ascher, 1997), we examined how intracellular Mg^{2+} affects the single channel amplitudes of

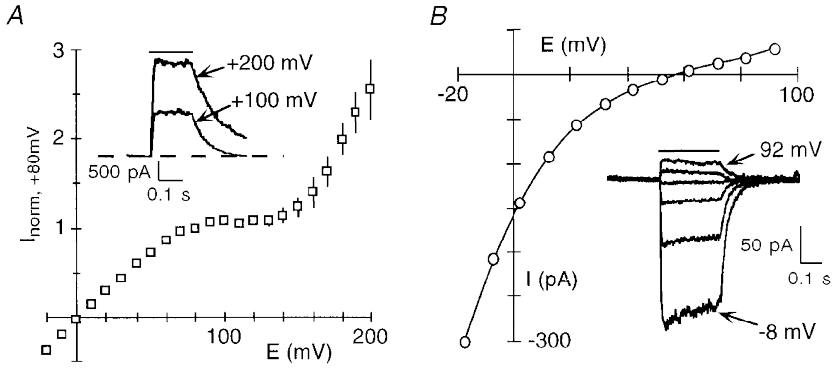

Figure 4. Intracellular Mg^{2+} permeates wild-type NR1–NR2A channels

A, mean peak current amplitudes recorded in HEK 293 cells with the pipette solution containing 0·3 mM Mg^{2+}. Individual records were normalized to their current amplitude at +80 mV to combine traces ($n = 4$ cells). Inset, glutamate-activated current at two different membrane potentials. The continuous line above the traces indicates application of glutamate (100 μM). Series resistance (R_S), 3·2 MΩ. *B*, peak current–voltage relationship for a HEK 293 cell with 80 mM $MgCl_2$ in the pipette and 103·5 mM KCl extracellularly. Inset, raw current records shown at 20 mV increments. R_S, 2·5 MΩ.

NR1(N0G) channels (Fig. 8). Figure 8*A* shows single channel activity at +50 mV, in the absence or presence of intracellular Mg^{2+} (1 mM) from an inside-out patch taken from a HEK 293 cell expressing NR1(N0G)–NR2A channels. In the absence of Mg^{2+} (upper trace), the single channel activity differed from wild-type in two respects. First, two distinct conductance levels were present, a main (O_m) and one subconductance (O_s) level. Second, the mean unitary amplitudes of both of these levels, 8·15 and 5·5 pA, respectively (Fig. 8*B*), were considerably larger than that of wild-type (~2·8 pA). The addition of 1 mM Mg^{2+} reduced the unitary amplitude of the main and sublevel to 5·37 and 3·55 pA, respectively (Fig. 8*C*), yielding a fraction blocked of, on average, $0{\cdot}36 \pm 0{\cdot}02$ and $0{\cdot}38 \pm 0{\cdot}02$, respectively ($n = 3$ patches). These values were indistinguishable from each other as well as from that obtained using macroscopic currents at the same potential ($0{\cdot}36 \pm 0{\cdot}02$, $n = 4$). Figure 8*D* illustrates the amplitudes of the main (open diamonds) and subconductance (filled diamonds) levels over a wide voltage range. Like wild-type, the slope conductance of the main conductance level was not symmetrical, being greater at potentials negative to the reversal potential (165 ± 4 pS) than at positive potentials (144 ± 1 pS, $n = 3$). On the other hand, the subconductance level differed from both the main and wild-type in showing a slight conductance asymmetry in the opposite direction, being 93 ± 2 pS at negative potentials and 105 ± 1 pS at positive potentials. The fraction blocked by 1 mM Mg^{2+} of the main (open diamonds) and subconductance (filled diamonds) levels is compared with that for wild-type (open circles) as well as for NR1(N0G) macroscopic currents (open squares) in Fig. 8*E*. At +70 mV, there was a divergence in the extent of block, with the subconductance level being more strongly blocked than the main, an effect we do not explore further here. Nevertheless, over physiological potentials, the fraction blocked for both the main and subconductance levels was indistinguishable from each other as well as from that measured using macroscopic currents. In addition, this block

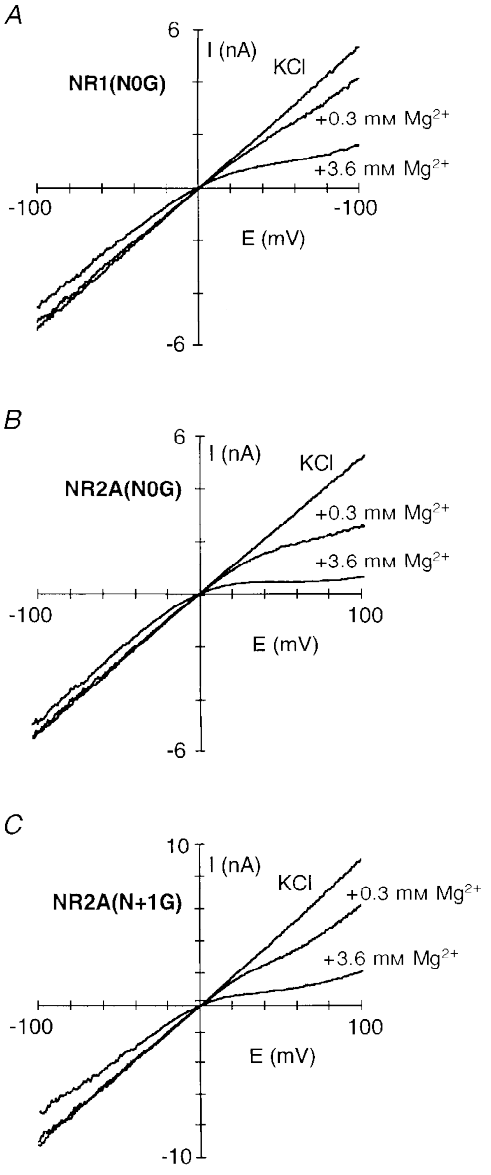

Figure 5. Intracellular Mg^{2+} block of glycine-substituted channels

Current traces for NR1(N0G)–NR2A (*A*), NR1–NR2A(N0G) (*B*) and NR1–NR2A(N + 1G) (*C*) channels recorded in the presence or absence of intracellular Mg^{2+} (0·3 or 3·6 mM). Traces recorded and displayed as in Fig. 1*A*.

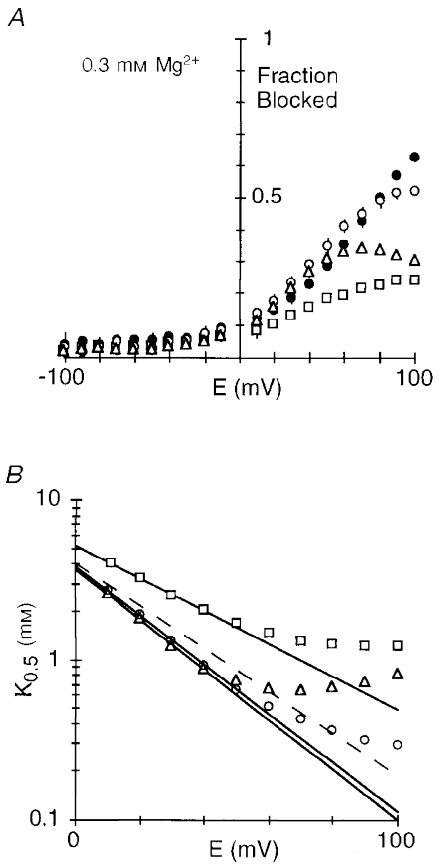

Figure 6. NR1(N0G) mutant channels have an attenuated block over the entire voltage range

A, mean fraction blocked, $1 - I_B/I_0$, in 0·3 mM Mg^{2+}. Each point is shown as the mean ± 2 S.E.M. ●, wild-type; □, NR1(N0G); ○, NR2A(N0G); △, NR2A(N + 1G). *B*, $K_{0.5}$ as a function of membrane potential, with the straight line a linear equation fit from: NR1(N0G) (□), +10 to +40 mV; NR2A(N0G) (○), +10 to +50 mV; and NR2A(N + 1G) (△), +10 to +40 mV. See Table 2 (NR1) and Table 3 (NR2A) for parameters. Dashed line is the same type of analysis for wild-type (Fig. 2*B*).

was attenuated compared with that found in wild-type channels, consistent with the idea that NR1(N0) contributes to a blocking site for intracellular Mg^{2+}.

We also quantified the reduction of single channel amplitudes in NR1–NR2A(N0G) and NR1– NR2A(N + 1G) channels (data not shown). NR2A(N0G) channels also showed two conductance levels (O_m, 7·3 ± 0·2 pA; and O_s, 5·3 ± 0·2 pA; $n = 4$). However, the subconductance level occurred infrequently, less than 10% of the total openings, and was of short duration. At +50 mV, the fraction blocked of the main conductance level by 1 mM Mg^{2+} was 0·60 ± 0·01, which was indistinguishable from that measured using macroscopic currents (0·60 ± 0·02, $n = 4$). NR2A(N + 1G) channels showed only a single conductance level with a mean unitary amplitude of 8·1 ± 0·1 pA ($n = 3$). The

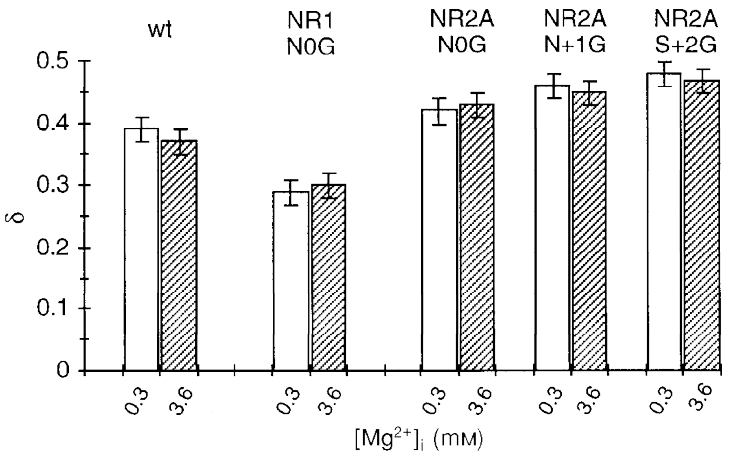

Figure 7. Voltage dependence of the block in glycine-substituted channels is not concentration dependent

Mean voltage dependence of the block, δ, in glycine-substituted channels. Values are shown as means ± 2 S.E.M. wt, wild-type.

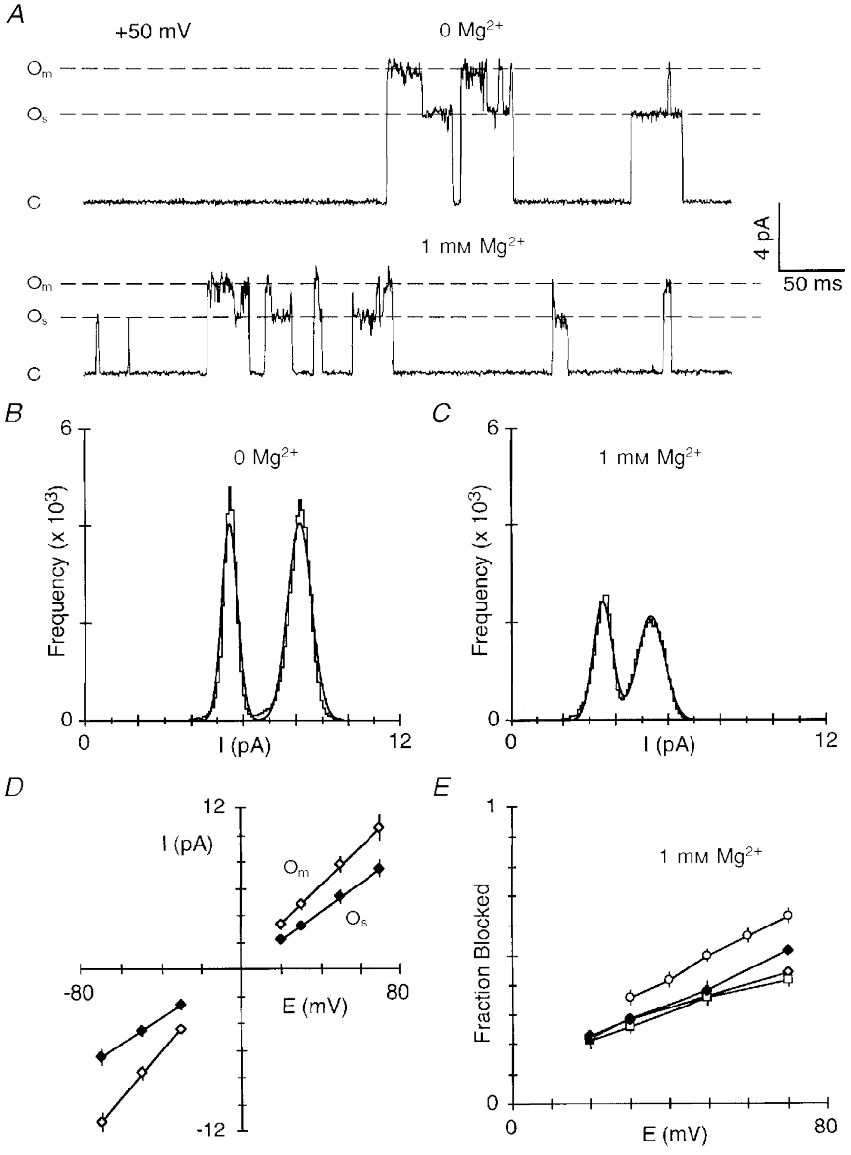

Figure 8. Block of single NR1(N0G)–NR2A channels by intracellular Mg^{2+} is reduced compared with wild-type

A, example single channel activity at +50 mV from an inside-out patch isolated from a HEK 293 cell expressing NR1(N0G)–NR2A channels. Activity was recorded in the absence (upper trace) or presence (lower trace) of 1 mM intracellular Mg^{2+}. O_m, main open conductance level; O_s, subconductance level; C, closed level. *B* and *C*, open point amplitude histograms in the absence (*B*) or presence (*C*) of 1 mM intracellular Mg^{2+} for the patch in *A*. Bin width was 0·1 pA. Continuous curves are fitted maximum likelihood Gaussian distributions. In 0 Mg^{2+}, the mean unitary amplitude for O_m was 8·15 ± 0·45 pA (mean ± S.D.) and for O_s it was 5·50 ± 0·30 pA; in 1 mM Mg^{2+}, O_m was 5·37 ± 0·50 pA and O_s was 3·55 ± 0·36 pA. In both the presence and absence of Mg^{2+}, the main conductance level represented about 55% of the total openings. *D*, mean unitary single channel current amplitudes as a function of voltage for the main (◇) and subconductance (◆) levels. Lines through the points are fitted linear equations yielding slope conductances for the main conductance level of 173 pS (negative limb) and 144 pS (positive limb) whereas for the subconductance level they were 96 pS (negative limb) and 107 pS (positive limb). *E*, mean fraction blocked, $1 - I_B/I_0$, in 1 mM Mg^{2+} for NR1(N0G) channels measured using macroscopic currents (□) or the reduction of single channel amplitudes for the main (◇) and subconductance (◆) levels. Each point is the mean of 3 patches except for those at +70 mV where only a single measurement was made. ○, wild-type (Fig. 3). Each point is shown as the mean ± 2 S.E.M. The lines have no theoretical significance.

fraction blocked of this amplitude at +50 mV by 1 mM Mg^{2+} was 0·57 ± 0·01, a value again indistinguishable from that measured using macroscopic currents (0·55 ± 0·01, $n = 5$).

In summary, the similarity between the reduction of single channel amplitudes and macroscopic currents by intracellular Mg^{2+} indicates that the block of macroscopic currents for the mutant channels primarily reflects an occlusion process, at least over intermediate potentials. These single channel results are also consistent with the idea that the substitution of glycine at NR1(N0) but not at NR2A(N0) or NR2A(N + 1) disrupts the block.

Substitution of glutamine for elements defining the narrow constriction alter the block by intracellular Mg^{2+}

The side chain glutamine (Q) differs from asparagine only in containing an added methylene group; hence, substitution of glutamine would alter the geometry of the side chains while leaving the amide side group intact. Figure 9 shows intracellular Mg^{2+} block in channels containing glutamine substituted for any one of the three asparagines. The extent of block in these mutant channels is compared with that in wild-type (filled circles) in Fig. 10*A*. In NR2A(N0Q) (open circles) the block was little affected over physiological potentials. Qualitatively, this action is similar to that observed for the glycine substitution and is consistent with the side chain at NR2A(N0) contributing little to a blocking site for intracellular Mg^{2+}. On the other hand, NR1(N0Q) (open squares) or NR2A(N + 1) (open triangles) channels produced stronger but opposite effects on the block. In the case of NR1(N0Q), the block was attenuated over the entire voltage range. In contrast, in NR2A(N + 1Q) the block was strongly enhanced (Table 3). This result contrasts with that for the glycine substitution at NR2A(N + 1) which suggested that this site contributes little to intracellular Mg^{2+} block over physiological potentials. To address

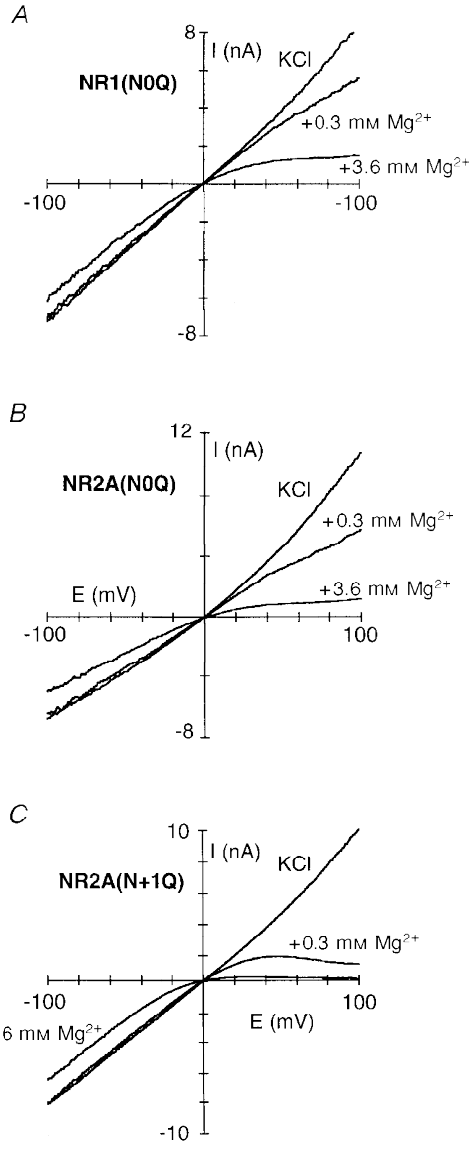

Figure 9. Intracellular Mg^{2+} block of glutamine-substituted channels

Current traces for NR1(N0Q)–NR2A (*A*), NR1–NR2A(N0Q) (*B*) and NR1–NR2A(N + 1Q) (*C*) channels recorded in the presence or absence of intracellular Mg^{2+} (0·3 or 3·6 mM). Traces recorded and displayed as in Fig. 1*A*.

further the contribution of the N + 1 site in the NR2A-subunit to the block, we examined double-mutant channels composed of NR2A(N + 1Q) co-expressed with glycine or serine substituted at NR1(N0). In both NR1(N0G)–NR2A(N + 1Q) and NR1(N0S)–NR2A(N + 1Q) channels, the block by intracellular Mg^{2+} was strongly attenuated (data not shown) and comparable to that for mutant channels containing substitutions only at NR1(N0). In 3·6 mM Mg^{2+}, for example, the fraction blocked at +50 mV in NR1(N0G)–NR2A(N + 1Q) or NR1(N0S)–NR2A(N + 1Q) was 49·0 ± 0·9 ($n = 4$) and 55·1 ± 0·6 ($n = 5$), respectively. These values were greatly attenuated compared with those for wild-type (78·1 ± 0·4) and NR1–NR2A(N + 1Q) (95·3 ± 0·3) but comparable to those for NR1(N0G)–NR2A (66·2 ± 0·4) and NR1(N0S)–NR2A (47·8 ± 1·5). Hence, while the NR2A(N + 1) site can influence intracellular Mg^{2+} block over physiogical potentials, NR1(N0) appears to make a more dominant contribution.

In summary, the G and Q substitutions suggest that elements defining the narrow constriction in NMDA receptor channels, the NR1(N0) and NR2A(N + 1) sites, contribute to a blocking site for intracellular Mg^{2+} but that the contribution by the NR1(N0) site is greater. In contrast, these same substitutions at NR2A(N0), which is apparently positioned externally to the narrow constriction, produced only weak effects on the block. To further define the contribution of residues forming the narrow constriction to the block, we compared intracellular Mg^{2+} block in channels containing other substitutions at NR1(N0) and NR2A(N + 1). Substitution of the negatively charged aspartate (D) at either NR1(N0) (Table 2) or NR2A(N + 1) (Table 3) enhanced the block to about an equivalent extent, consistent with intracellular Mg^{2+} interacting with this region. The block in NR1(N0D) channels was also concentration dependent (Table 2), an effect we do not explore further here but again suggesting a differential contribution of these two positions to the block. Substitution of the polar serine (S) at either NR1(N0) or NR2A(N + 1) produced very different effects on the block by intracellular Mg^{2+} as well as that by extracellular Mg^{2+} and we considered them in more detail.

Intracellular Mg^{2+} interacts differently with residues defining the narrow constriction

Figure 11 shows intracellular Mg^{2+} block in channels containing serine substituted at either NR1(N0) (Fig. 11*A*) or NR2A(N + 1) (Fig. 11*B*). A direct comparison of the fraction blocked in these mutant channels with that in wild-type (filled circles) is shown in Fig. 11*C*. The block in NR2A(N + 1S) was strongly altered only at very positive potentials and qualitatively gave a similar response to the glycine substitution (Table 3). In contrast, in NR1(N0S) the extent of block as well as the voltage dependence of it was strongly attenuated. The block over a wide concentration range in NR1(N0S) is quantified in Fig. 11*D*. Two distinct linear regions of block were discernible. Over physiological potentials (+10 to +50 mV), the voltage dependence of the block was strongly reduced to about 0·13, as was $K_{0.5}$(0 mV) to 5·1 mM. At more positive potentials (+80 to +140 mV), a stronger voltage-dependent component (0·28) was found,

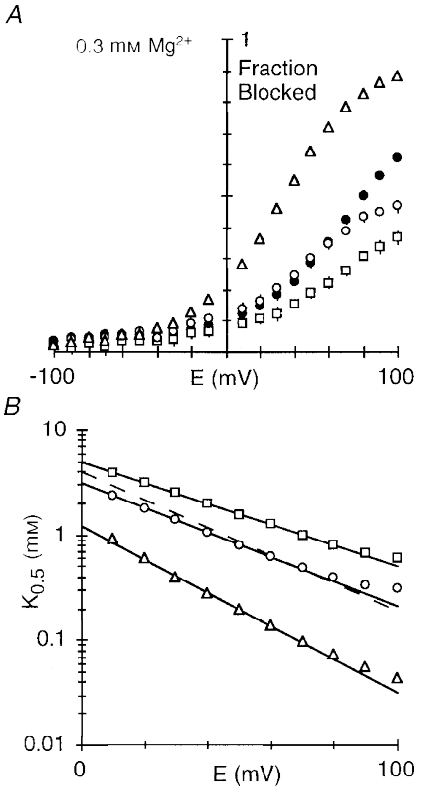

Figure 10. Voltage dependence of the block in glutamine-substituted channels

A, mean fraction blocked, $1 - I_B/I_0$, in 0·3 mM Mg^{2+}. Each point is shown as the mean ± 2 S.E.M. ●, wild-type; □, NR1(N0Q); ○, NR2A(N0Q); △, NR2A(N + 1Q). *B*, $K_{0.5}$ as a function of membrane potential, with the straight line a linear equation fit from: NR1(N0Q) (□), +10 to +70 mV; NR2A(N0Q) (○), +10 to +60 mV; and NR2A(N + 1Q) (△), +10 to +70 mV. See Table 2 (NR1) and Table 3 (NR2A) for parameters. Dashed line is wild-type (Fig. 2*B*).

Table 2. Woodhull parameters for intracellular Mg^{2+} block of NMDA receptor channels containing mutant NR1-subunits

Subunit composition	$[Mg^{2+}]$ (mM)	δ	$K_{0.5}$(0 mV) (mM)	n
NR1(N0G)–NR2A	0·1–20	0·30 ± 0·01	5·2 ± 0·1	6
NR1(N0S)–NR2A	0·1–20	0·13 ± 0·01	5·1 ± 0·1	8
NR1(N0Q)–NR2A	0·1–20	0·29 ± 0·01	5·1 ± 0·1	6
NR1(N0D)–NR2A	0·3	0·37 ± 0·01	1·8 ± 0·1	6
	3·6	0·44 ± 0·01	2·2 ± 0·1	6
NR1(N0R)–NR2A	3·6	—*	—*	3

See Table 1 for solutions. Ranges of concentrations were fitted using eqn (3) whereas individual concentrations were fitted using eqn (2). Fitted ranges were typically from +10 to +60 mV. * The current was blocked by less than 10 % at all potentials. Values are means ± S.E.M.

Table 3. Woodhull parameters for intracellular Mg^{2+} block of NMDA receptor channels containing mutant NR2A-subunits

Subunit composition	$[Mg^{2+}]$ (mM)	δ	$K_{0.5}$(0 mV) (mM)	n
NR1–NR2A(N0G)	0·1–20	0·45 ± 0·01	3·9 ± 0·1	4
NR1–NR2A(N0Q)	0·1–20	0·34 ± 0·01	3·1 ± 0·1	4
NR1–NR2A(N + 1G)	0·1–20	0·46 ± 0·01	3·8 ± 0·1	10
NR1–NR2A(N + 1S)	0·3; 3·6	0·38 ± 0·02	3·0 ± 0·2	5
NR1–NR2A(N + 1Q)	0·05–3·6	0·47 ± 0·02	1·3 ± 0·1	5
NR1–NR2A(N + 1D)	0·3; 3·6	0·36 ± 0·01	2·2 ± 0·2	4
NR1–NR2A(S + 2G)	0·3; 3·6	0·47 ± 0·01	2·3 ± 0·1	5

See Table 1 for solutions. Ranges of concentrations were fitted using eqn (3) whereas individual concentrations were fitted using eqn (2). Fitted ranges were typically from +10 to +60 mV. Values are means ± S.E.M.

which exhibited a low affinity (11·6 mM). How the serine substitution alters the block is unknown but it appears that at least part of the mechanism may be that only at extreme potentials is Mg^{2+} able to enter deep into the pore. Consistent with this idea is that NR1(N0S) channels have a strongly attenuated intracellular and extracellular Mg^{2+} permeability (see Fig. 14*B*). This is supported by the observation that at very positive potentials the block in NR1(N0S) is linear rather than deviating upward as seen in wild-type, a response we have interpreted as reflecting Mg^{2+} permeation.

Extracellular and intracellular Mg^{2+} interact differently with structural determinants of the narrow constriction

Substitutions at NR1(N0) or NR2A(N + 1), residues which contribute to the narrow constriction, altered the block by intracellular or extracellular Mg^{2+} to varying degrees. Figure 12 shows a direct comparison of intracellular and extracellular Mg^{2+} block for mutant channels containing serine substituted at either NR1(N0) (Fig. 12*A*) or NR2A(N + 1) (Fig. 12*B*); these mutant channels were selected for comparison since they produced the strongest disruption of the block by intracellular (NR1(N0S)) or extracellular (NR2A(N + 1S)) Mg^{2+}. In NR1(N0S) the block by intracellular Mg^{2+} (Fig. 12*A*, left panel) was severely disrupted reducing both the voltage dependence and the $K_{0.5}$(0 mV). In contrast, the block by extracellular Mg^{2+} was little changed (Fig. 12*A*, right panel) giving an indistinguishable voltage dependence ($\delta \approx 0{\cdot}80$ compared with 0·82 for wild-type) and an enhanced voltage-independent affinity (1·3 compared with 4·1 mM) (Wollmuth *et al.* 1998). On the other hand, in NR2A(N + 1S) the block by intracellular Mg^{2+} was attenuated only at extremely positive potentials (Fig. 12*B*, left panel) whereas the block by extracellular Mg^{2+} was attenuated over the entire voltage range. Hence, for intracellular Mg^{2+}, the asparagine at the NR1-subunit N-site contributes to a blocking site over physiological potentials with the NR2A-subunit N + 1 site contributing little. For extracellular Mg^{2+}, an opposite pattern appears to hold.

Residues at the narrow constriction form a barrier for Mg^{2+} permeability

To distinguish further how residues positioned at or near the narrow constriction interact with intracellular and extracellular Mg^{2+}, we compared reversal potentials measured in high intracellular Mg^{2+} to those measured in high extracellular Mg^{2+} for these mutant channels. These measures are of limited quantitative value (see Methods) but provide additional evidence that intracellular and extracellular Mg^{2+} interact with different determinants of the narrow constriction.

Figure 13 shows current reversals with 80 mM Mg^{2+} in the pipette for mutant channels containing glycine substituted for any one of the three asparagines. For all three mutant channels, the reversal potential relative to wild-type (arrows) was shifted towards zero indicating an increased apparent Mg^{2+} permeability. These changes in the apparent Mg^{2+} permeability differ from that for extracellular Mg^{2+}. Figure 14*A* shows a direct comparison of Mg^{2+} reversal potentials measured in high intracellular or extracellular Mg^{2+} for the glycine substitutions, with the results shown as $E_{r(wild)}/E_{r(mutant)}$ (E_r, reversal potential); in this form, an increase in the reversal potential relative to wild-type will give a value greater than unity whereas a decrease will give a value less than unity. The most striking difference occurred with the NR1(N0G) substitution which produced an opposite effect on the apparent reversal potential, increasing it from the intracellular side and decreasing it from the extracellular side (Fig. 14*A*). On the other hand, the NR2A(N0G) or NR2A(N + 1G) substitutions increased the reversal potentials measured either from the intracellular or extracellular side. A comparison of reversal potentials measured with high intracellular or extracellular Mg^{2+} for other substitutions of the three asparagines (Fig. 14*B*) confirmed this finding. Hence, all three asparagines contribute to the barrier for Mg^{2+} permeation from the intracellular side. This contrasts with extracellular Mg^{2+} where the two adjacent asparagines in the NR2-subunit contributed to the barrier whereas the N-site asparagine in the NR1-subunit did not (Wollmuth *et al.* 1998).

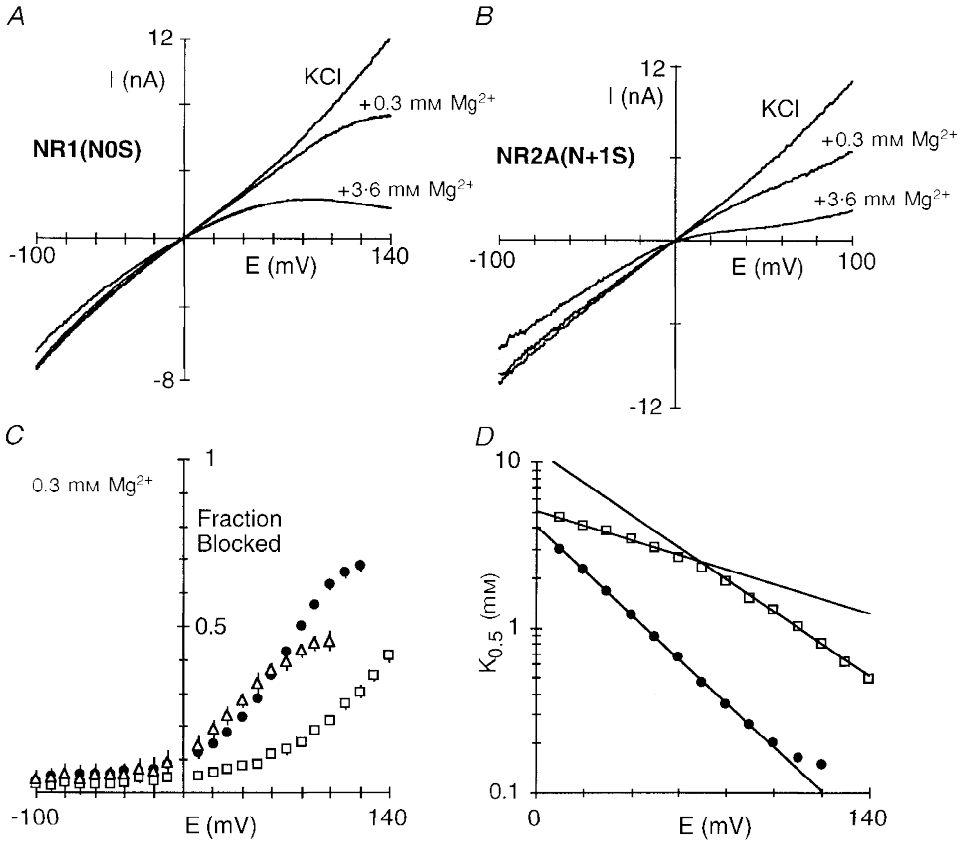

Figure 11. Intracellular Mg^{2+} interacts differently with elements defining the narrow constriction

Current traces for NR1(N0S)–NR2A (*A*) and NR1–NR2A(N + 1S) (*B*) channels recorded in the presence or absence of intracellular Mg^{2+}. Traces recorded and displayed as in Fig. 1*A*. *C*, mean fraction blocked, $1 - I_B/I_0$, in 0·3 mM Mg^{2+}. Each point is shown as the mean ± 2 S.E.M. ●, wild-type; □, NR1(N0S); △, NR2A(N + 1S). *D*, $K_{0.5}$ as a function of membrane potential for NR1(N0S) (□), with the straight lines a linear equation fit giving parameters of δ and $K_{0.5}$(0 mV), respectively, of 0·28 ± 0·01 and 11·6 ± 0·8 mM (+80 to +140 mV; $n = 8$) and 0·13 ± 0·01 and 5·1 ± 0·1 mM (+10 to +50 mV). ●, wild-type (Fig. 2*B*).

DISCUSSION

Residues that form the narrow constriction in NMDA receptor channels are positioned very near each other, presumably within 0·55 nm, the diameter of the narrow constriction (Villarroel *et al.* 1995; Zarei & Dani, 1995; Wollmuth *et al.* 1996). Substitutions of the native residues by other amino acids can have strong effects on Ca^{2+} permeability (Burnashev *et al.* 1992) as well as single channel properties (e.g. Premkumar & Auerbach, 1996; Schneggenburger & Ascher, 1997; Fig. 8). To identify how residues that form the narrow constriction contribute to intracellular Mg^{2+} block, we measured the block in the absence of Ca^{2+} (10 mM EDTA extracellularly), tested a wide range of Mg^{2+} concentrations, determined single channel amplitudes, and investigated several amino acid substitutions at a single position, anticipating that if a side chain contributes to the block, a side chain-dependent pattern of block should be seen. We conclude that intracellular Mg^{2+} interacts with residues forming the narrow constriction, with the N-site asparagine of the NR1-subunit representing the primary blocking site over physiological membrane potentials. This differs from extracellular Mg^{2+} where the two adjacent asparagines of the NR2A-subunit underlie the block with the N-site asparagine in the NR1-subunit contributing little.

Intracellular Mg^{2+} block of wild-type NMDA receptor channels

In wild-type, we found three distinct voltage ranges for the block by intracellular Mg^{2+}. Between +10 and +80 mV the block followed a simple Woodhull model. Over this range, permeation of Mg^{2+} does not appear to modify the block significantly since the block parameters, δ and $K_{0.5}$(0 mV), were concentration independent (Table 1; see also Li-Smerin & Johnson, 1996*a*). On the other hand, at potentials positive to +80 mV, the block was weaker than that expected, presumably reflecting the fact that, at these extreme potentials, permeation became significant. Finally, at potentials negative to 0 mV, the block was stronger than that expected. This additional component suggests that Mg^{2+} interacts with a site near the intracellular mouth of the channel. This additional component, however, is not present at low Mg^{2+} concentrations. Since the block parameters measured at positive potentials were independent of Mg^{2+} concentration, this additional site is presumably not occupied when Mg^{2+} blocks the channel at the deeper site. Consistent with this idea is that NMDA receptor channels appear to contain only a single Mg^{2+} ion (Zarei & Dani, 1994).

Prior reports on intracellular Mg^{2+} block of native NMDA receptor channels, which was measured using single channel

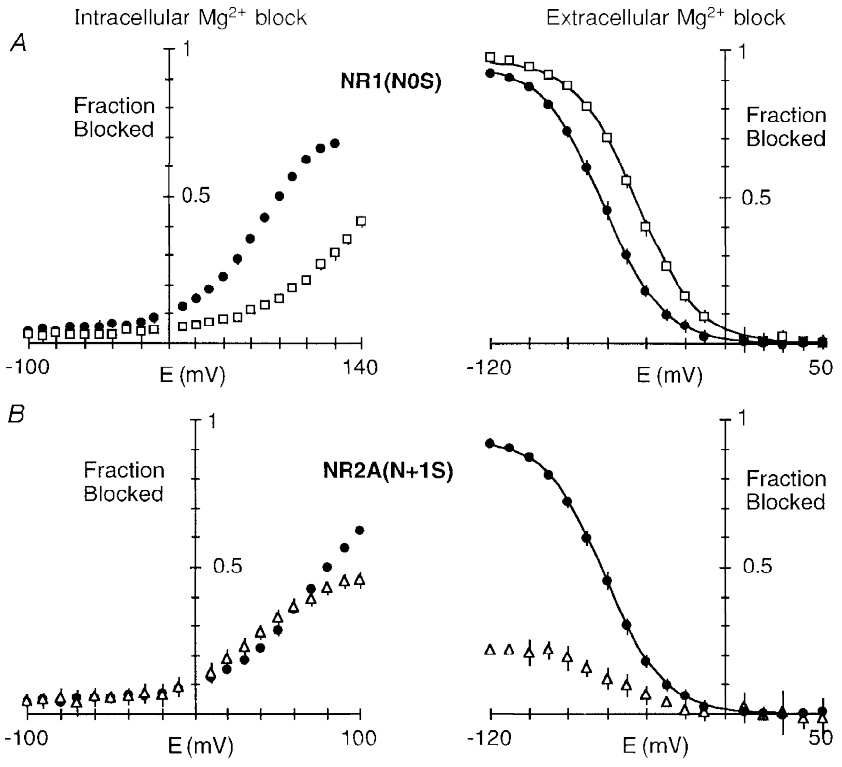

Figure 12. Intracellular and extracellular Mg^{2+} interact with different elements of the narrow constriction

Mean fractional block for NR1(N0S)–NR2A (*A*) and NR1–NR2A(N + 1S) (*B*) channels by intracellular (left panel) or extracellular (right panel) Mg^{2+}. Wild-type are shown as filled symbols. The Mg^{2+} concentration was 0·3 mM (intracellular) or 0·07 mM (extracellular). Data for extracellular Mg^{2+} block are from the companion paper (Wollmuth *et al.* 1998).

amplitudes and with Ca^{2+} extracellularly, show similarities and differences to our results. The voltage dependence of the block ($\delta \approx 0{\cdot}35$; Johnson & Ascher, 1990) is comparable to our values (0·36–0·39; Table 1). However, the voltage-independent affinity was lower (~8 mM) compared with 4 mM in our study and no significant inhibition of the current by intracellular Mg^{2+} occurred at negative potentials. These differences appear to be related to the fact that we made measurements in the absence of extracellular Ca^{2+}. Indeed, in the presence of extracellular Ca^{2+}, the block is weaker (L. P. Wollmuth & T. Kuner, unpublished data). In addition, we found that the NR1-subunit N-site is a critical determinant of intracellular Mg^{2+} block but that this site is also an important determinant of Ca^{2+} permeation (Burnashev *et al.* 1992). Hence, extracellular Ca^{2+} may attenuate intracellular Mg^{2+} block; conversely, intracellular Mg^{2+} may influence Ca^{2+} transport by directly competing with a site critical for inward Ca^{2+} flux as well as possibly influencing the ability of Ca^{2+} to enter the pore via an electrostatic mechanism.

An additional difference from prior reports is that we found no apparent effect of intracellular Mg^{2+} on channel gating (cf. Li-Smerin & Johnson, 1996*b*). Presumably, if intracellular Mg^{2+} increases the open probability of the channels as well as reducing their amplitude, the net effect at the macroscopic level should be an attenuated block compared with that for the reduction of single channel amplitudes. Nevertheless, the block of macroscopic currents was indistinguishable from that measured using the reduction of single channel current amplitudes (Fig. 3). The basis for the lack of a clear effect on channel gating is unknown but three possibilities can be considered. First, it may be dependent on the presence of extracellular Ca^{2+}. Second, it may be an NR2A-subunit specific action as all of our results are based on the NR2A-subunit. In the study of Li-Smerin & Johnson (1996*a*), the

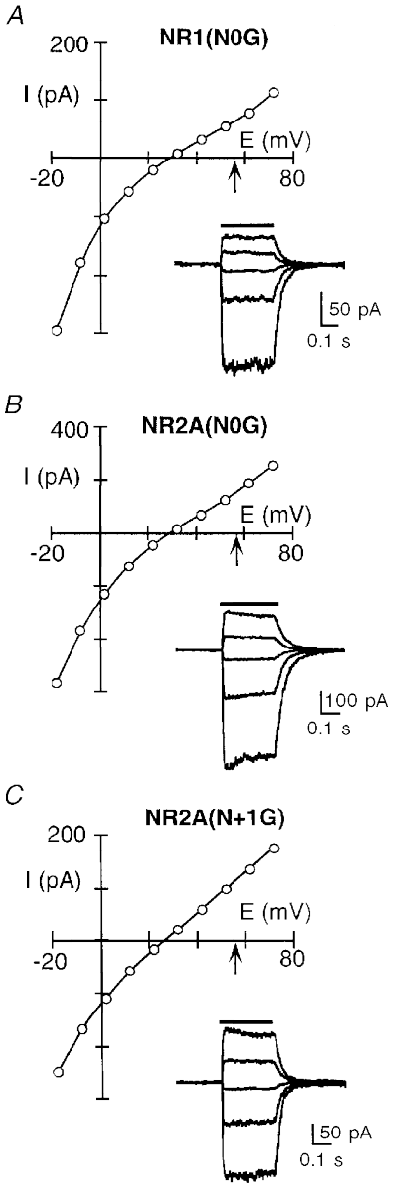

Figure 13. Apparent intracellular Mg^{2+} permeability in glycine-substituted channels

Glutamate-activated currents, with 80 mM $MgCl_2$ in the pipette, in HEK 293 cells expressing NR1(N0G)–NR2A (*A*), NR1–NR2A(N0G) (*B*) or NR1–NR2A(N + 1G) (*C*) channels. The arrow in each trace indicates the mean reversal potential for wild-type. Insets, raw current records shown at 20 mV increments.

amplitude and kinetics of the single channels are compatible with either NR1–NR2A or NR1–NR2B recombinant channels (Stern, Béhé, Schoepfer & Colquhoun, 1992). Finally, the Mg^{2+}-dependent increase in open probability may act through accessory proteins or the cytoskeleton, which may not be present in oocytes or HEK 293 cells.

The N-site asparagine in the NR1-subunit contributes to a blocking site for intracellular Mg^{2+}

The homologous N-site asparagines in the NR1- and NR2A-subunits are positioned at the tip of the loops formed by the M2 segments. However, the narrowest part of the channel is formed primarily by the asparagines at the N-site in the NR1-subunit and the N + 1 site in the NR2A-subunit, with the NR2-subunit N-site positioned externally (Kuner *et al.* 1996; Wollmuth *et al.* 1996). The present results suggest that intracellular Mg^{2+} interacts with amino acid residues forming the narrow constriction. However, based on the pattern of block over the entire voltage range and on different substitutions at each position, we conclude that the NR1-subunit N-site asparagine represents the primary structural determinant of the blocking site. At NR1(N0) but not at NR2A(N + 1), substitution of glycine, which would remove any structural or energetic contribution a side chain would make to block, resulted in channels where the block was attenuated over the entire voltage range (Fig. 6). A similar result was found when serine was substituted at either position (Fig. 11). In addition, the NR1(N0G) substitution induced two distinct single channel conductance levels, yet at least over physiological potentials their amplitudes were affected equally by intracellular Mg^{2+} and to the same extent as macroscopic currents.

Substitutions at NR1(N0), however, did not produce large changes in the block. This is not unexpected given the rapid flickering block seen at the single channel level (Johnson & Ascher, 1990; Li-Smerin & Johnson, 1996*a*). Indeed, in Fig. 3*A* the blocking events were too rapid to resolve and were manifested as a reduced single channel amplitude suggesting that any direct interaction between intracellular Mg^{2+} and the channel (binding) is not strong. Hence, intracellular Mg^{2+} may block NMDA receptor channels in a highly hydrated state, losing perhaps only one or two waters of its sixfold hydration shell (see Fig. 15). Consistent with this idea is that the extent of the block at extreme potentials (+100 mV) parallels the effect substitutions, especially at NR2A(N + 1), have on the size of the narrow constriction (data not shown). Also, although other structural elements presumably in the M2 segment contribute to the energetic profile that intracellular Mg^{2+} experiences (e.g. Kupper, Ascher & Neyton, 1996), given that the NR1-subunit N-site is positioned near the tip of the loop and substitutions of it increase the apparent permeation of intracellular Mg^{2+}, it appears to represent the deepest point in the channel for block by intracellular Mg^{2+}.

Substitution of glycine for either of the adjacent asparagines in the NR2A-subunit disrupted intracellular Mg^{2+} block only at very positive potentials. This disruption occurred at a less positive potential with NR2A(N + 1G) than with NR2A(N0G) substitutions (Fig. 6*B*). Our interpretation of this is that intracellular Mg^{2+} interacts with the NR1-subunit N-site over physiological potentials but with increasingly positive potentials, Mg^{2+} ions are pushed deeper into the narrow constriction interacting first with the NR2A-subunit N + 1 site and then at very positive potentials with the NR2A-subunit N-site. This pattern is consistent with the idea that the N-site in the NR2A-subunit is positioned externally to the narrow constriction formed by NR1(N0) and NR2A(N + 1) (Kuner *et al.* 1996).

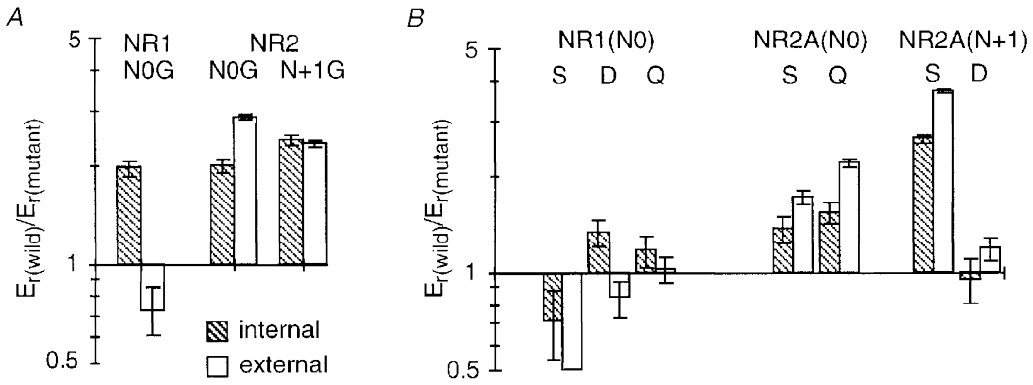

Figure 14. Substitutions of residues positioned at or near the narrow constriction alter the apparent efflux by intracellular Mg^{2+}

A and *B*, mean Mg^{2+} reversal potentials measured with high intracellular or extracellular Mg^{2+} for mutant NMDA receptor channels plotted relative to that for wild-type. Reversal potentials for NR2A(N + 1Q) channels could not be determined because the outwardly directed current was too small, and for NR2A(N0D) it was not analysed (see Wollmuth *et al.* 1998). Data for extracellular Mg^{2+} are from the companion paper (Wollmuth *et al.* 1998).

In addition, given that substitutions at NR2A(N0), which does not participate in the block, increased the apparent Mg^{2+} permeability suggests that sites removed from the blocking site can influence permeation. Nevertheless, an increase in the apparent Mg^{2+} permeability did not attenuate the block over physiological potentials (e.g. NR2A(N0G) and NR2A(N + 1G)). Presumably, this reflects the fact that the barrier for the return of Mg^{2+} to the intracellular side is much lower than the barrier for Mg^{2+} to traverse the channel even when this latter barrier is significantly lowered (see Li-Smerin & Johnson, 1996*a*).

Intracellular and extracellular Mg^{2+} interact with different amino acid side chains at the narrow constriction in NMDA receptor channels

A Woodhull model describes the block by both intracellular and extracellular Mg^{2+} quite well over an intermediate range of membrane potentials (Fig. 2*B*; see Wollmuth *et al.* 1998). Like prior reports, the block by extracellular Mg^{2+}, measured under identical ionic conditions, shows a stronger voltage dependence ($\delta \approx 0{\cdot}80$) but a comparable $K_{0{\cdot}5}$(0 mV) (~4 mM). However, Li-Smerin & Johnson (1996*a*), studying native NMDA receptor channels, suggested that the block by intracellular and extracellular Mg^{2+} is mediated by different sites in the channel. Our results are consistent with this view, specify residues that are responsible for this difference and indicate a subunit specificity to the different blocking sites. For intracellular Mg^{2+}, a residue in the NR1-subunit, the N-site asparagine, is a major determinant of the block, as illustrated in Fig. 15. In contrast, for extracellular Mg^{2+}, the block is determined by residues in the NR2A-subunit, the N-site, and more importantly by the N + 1 site asparagines (see Fig. 13 of Wollmuth *et al.* 1998). Thus, different structural elements contribute to the block by intracellular and extracellular Mg^{2+}. Nevertheless, these two blocking sites appear to be positioned close together, presumably within 0·55 nm, the diameter of the narrow constriction.

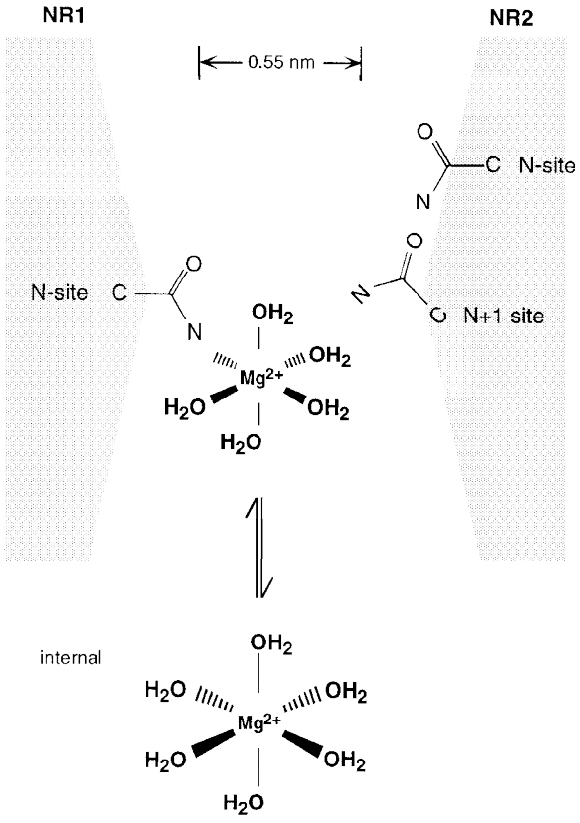

Figure 15. The N-site asparagines in the NR1-subunit contribute to a blocking site for intracellular Mg^{2+}

Schematic drawing of amino acid residues positioned at or near the narrow constriction. Mg^{2+} prefers an octahedral (sixfold) co-ordination. In solution, the co-ordination spheres are occupied by water. In the pore, bound Mg^{2+} loses anywhere from 1 to 6 waters of hydration with the free electron pairs in the carbonyl oxygen and/or amide nitrogen of the asparagine side chain substituting for the water molecules. The effective diameter of hydrated Mg^{2+}, which is not drawn to scale, is at least 0·7 nm considering only the primary hydration shell and assigning a diameter of 0·28 nm to a water molecule and 0·13 nm to Mg^{2+} (Frausto da Silva & Williams, 1991).

How the structural elements of the narrow constriction distinguish between intracellular and extracellular Mg^{2+} remains unknown. Indeed, none of the side chains at the narrow constriction are positioned identically with respect to the vertical channel axis, being staggered relative to each other (see Fig. 1*B* of Wollmuth *et al.* 1998). A pentameric subunit stoichiometry composed of different types of subunits (NR1 and NR2) would suggest, in addition, an asymmetrical positioning of sites in the horizontal plane of the narrow constriction. Consistent with this view is that the narrow constriction may be rectangular in shape (Zarei & Dani, 1995). Thus, different geometries of the intracellular and extracellular vestibules may guide Mg^{2+} to interact with different parts of the narrow constriction.

Residues forming the narrow constriction in NMDA receptor channels are accessible to ions from both sides of the membrane and are critical for extracellular Mg^{2+} block (NR2(N0), NR2(N + 1)) (Burnashev *et al.* 1992; Mori *et al.* 1992; Wollmuth *et al.* 1998), Ca^{2+} permeation (NR1(N0)) (Burnashev *et al.* 1992), and as shown here, intracellular Mg^{2+} block (NR1(N0)). Based on the voltage dependence of the block by intracellular Mg^{2+}, the narrow constriction in wild-type channels appears to be positioned about 40 % of the way across the electric field from the intracellular side, in agreement with the block by intracellular organic cations (Villarroel *et al.* 1995; Zarei & Dani, 1995). Given this positioning of the narrow constriction, the strong voltage dependence of the block by extracellular Mg^{2+} ($\delta \approx 0{\cdot}80$) cannot arise by a single Mg^{2+} blocking the channel at the narrow constriction. The possibility that the position of side chains at the interface to the lumen of the channel depends on membrane potential, with the narrow constriction moving with the electric field, should be considered.

Ascher, P. & Nowak, L. (1988). The role of divalent cations in the *N*-methyl-D-aspartate responses of mouse central neurones in culture. *Journal of Physiology* **399**, 247–266.

Bliss, T. V. P. & Collingridge, G. L. (1993). A synaptic model of memory: long-term potentiation in the hippocampus. *Nature* **361**, 31–39.

Burnashev, N., Schoepfer, R., Monyer, H., Ruppersberg, J. P., Günther, W., Seeburg, P. H. & Sakmann, B. (1992). Control by asparagine residues of calcium permeability and magnesium blockade in the NMDA receptor. *Science* **257**, 1415–1419.

DiFrancesco, D. (1982). Block and activation of the pacemaker channel in calf purkinje fibres: effects of potassium, caesium and rubidium. *Journal of Physiology* **329**, 485–507.

Frausto da Silva, J. J. R. & Williams, R. J. P. (1991). *The Biological Chemistry of the Elements*, 1st edn. Clarendon Press, Oxford.

Hilgemann, D. W. (1995). The giant membrane patch. In *Single-Channel Recordings*, 2nd edn, ed. Sakmann, B. & Neher, E., pp. 307–327. Plenum Press, New York.

Jahr, C. E. & Stevens, C. F. (1990). A quantitative description of NMDA receptor–channel kinetic behavior. *Journal of Neuroscience* **10**, 1830–1837.

Johnson, J. W. & Ascher, P. (1990). Voltage-dependent block by intracellular Mg^{2+} of *N*-methyl-D-aspartate channels. *Biophysical Journal* **57**, 1085–1090.

Kuner, T., Wollmuth, L. P., Karlin, A., Seeburg, P. H. & Sakmann, B. (1996). Structure of the NMDA receptor channel M2 segment inferred from the accessibility of substituted cysteines. *Neuron* **17**, 343–352.

Kupper, J., Ascher, P. & Neyton, J. (1996). Probing the pore region of recombinant *N*-methyl-D-aspartate channels using external and internal magnesium block. *Proceedings of the National Academy of Sciences of the USA* **93**, 8648–8653.

Li-Smerin, Y. & Johnson, J. W. (1996*a*). Kinetics of the block by intracellular Mg^{2+} of the NMDA-activated channel in cultured rat neurons. *Journal of Physiology* **491**, 121–135.

Li-Smerin, Y. & Johnson, J. W. (1996*b*). Effects of intracellular Mg^{2+} on channel gating and steady-state responses of the NMDA receptor in cultured rat neurons. *Journal of Physiology* **491**, 137–150.

Moisescu, D. G. & Thieleczek, R. (1978). Calcium and strontium concentration changes within skinned muscle preparations following a change in the external bathing solution. *Journal of Physiology* **275**, 241–262.

Mori, H., Masaki, H., Yamakura, T. & Mishina, M. (1992). Identification by mutagenesis of a Mg^{2+}-block site of the NMDA receptor channel. *Nature* **358**, 673–675.

Nowak, L. M. & Wright, J. M. (1992). Slow voltage-dependent changes in channel open-state probability underlie hysteresis of NMDA responses in Mg^{2+}-free solutions. *Neuron* **8**, 181–187.

Premkumar, L. S. & Auerbach, A. (1996). Identification of a high affinity divalent cation binding site near the entrance of the NMDA receptor channel. *Neuron* **16**, 869–880.

Sakurada, K., Masu, M. & Nakanishi, S. (1993). Alteration of Ca^{2+} permeability and sensitivity to Mg^{2+} and channel blockers by a single amino acid substitution in the *N*-methyl-D-aspartate receptor. *Journal of Biological Chemistry* **268**, 410–415.

Schneggenburger, R. & Ascher, P. (1997). Coupling of permeation and gating in an NMDA-channel pore mutant. *Neuron* **18**, 167–177.

Stephenson, D. G. & Thieleczek, R. (1986). Activation of the contractile apparatus of skinned fibres of frog by the divalent cations barium, cadmium and nickel. *Journal of Physiology* **380**, 75–92.

Stern, P., Béhé, P., Schoepfer, R. & Colquhoun, D. (1992). Single-channel conductances of NMDA receptors expressed from cloned cDNAs: Comparison with native receptors. *Proceedings of the Royal Society* B **250**, 271–277.

Villarroel, A., Burnashev, N. & Sakmann, B. (1995). Dimensions of the narrow portion of a recombinant NMDA receptor channel. *Biophysical Journal* **68**, 866–875.

Wollmuth, L. P. (1994). Mechanism of Ba^{2+} block of M-like K channels of rod photoreceptors of tiger salamanders. *Journal of General Physiology* **103**, 45–66.

Wollmuth, L. P., Kuner, T. & Sakmann, B. (1998). Adjacent asparagines in the NR2A-subunit of the NMDA receptor channel control the voltage-dependent block by extracellular Mg^{2+}. *Journal of Physiology* **506**, 13–32.

Wollmuth, L. P., Kuner, T., Seeburg, P. H. & Sakmann, B. (1996). Differential contribution of the NR1- and NR2A-subunits to the selectivity filter of recombinant NMDA receptor channels. *Journal of Physiology* **491**, 779–797.

Woodhull, A. M. (1973). Ionic blockage of sodium channels in nerve. *Journal of General Physiology* **61**, 687–708.

Zarei, M. M. & Dani, J. A. (1994). Ionic permeability characteristics of the *N*-methyl-D-aspartate receptor channel. *Journal of General Physiology* **103**, 231–248.

Zarei, M. M. & Dani, J. A. (1995). Structural basis for explaining open-channel blockade of the NMDA receptor. *Journal of Neuroscience* **15**, 1446–1454.

Acknowledgements

We thank Peter H. Seeburg for his generous support, H. Spiegel for expert secretarial assistance, and M. Kaiser and S. Grünewald for technical assistance. D. Feldmeyer is also thanked for assistance in measuring single channel currents, and D. Colquhoun (University College London, UK) for the single channel analysis software. This work was supported in part by a long-term Human Frontier Science Fellowship (L.P.W.).

Corresponding author

L. P. Wollmuth: Abteilung Zellphysiologie, Max-Planck-Institut für medizinische Forschung, Jahnstrasse 29, D-69120 Heidelberg, Germany.

Email: wollmuth@sunny.mpimf-Heidelberg.mpg.de